



Article

# Energy and Exergy Analysis of Using Turbulator in a Parabolic Trough Solar Collector Filled with Mesoporous Silica Modified with Copper Nanoparticles Hybrid Nanofluid

Sara Rostami <sup>1,2</sup>, Amin Shahsavari <sup>3,\*</sup>, Gholamreza Kefayati <sup>4,\*</sup> and Aysan Shahsavari Goldanlou <sup>5,6</sup>

<sup>1</sup> Laboratory of Magnetism and Magnetic Materials, Advanced Institute of Materials Science, Ton Duc Thang University, Ho Chi Minh City, Vietnam; sara.rostami@tdtu.edu.vn

<sup>2</sup> Faculty of Applied Sciences, Ton Duc Thang University, Ho Chi Minh City, Vietnam

<sup>3</sup> Department of Mechanical Engineering, Kermanshah University of Technology, Kermanshah 6715685420, Iran

<sup>4</sup> School of Engineering, University of Tasmania, Hobart, Tasmania 7005, Australia

<sup>5</sup> Institute of Research and Development, Duy Tan University, Da Nang 550000, Vietnam; aysanshahsavargoldanlou@duytan.edu.vn

<sup>6</sup> Faculty of Electrical—Electronic Engineering, Duy Tan University, Da Nang 550000, Vietnam

\* Correspondence: a.shahsavari@kut.ac.ir (A.S.); gholamreza.kefayati@utas.edu.au (G.K.)

Received: 6 May 2020; Accepted: 3 June 2020; Published: 8 June 2020



**Abstract:** Designing the most efficient parabolic trough solar collector (PTSC) is still a demanding and challenging research area in solar energy systems. Two effective recommended methods for this purpose that increase the thermal characteristics of PTSCs are adding turbulators and nanofluids. To study the effects of the two approaches on the energy efficiency of PTSCs, a stainless steel turbulator was used and solid nanoparticles of Cu/SBA-15 were added to the water with the volume concentrations of 0.019% to 0.075%. The generated turbulence in the fluid flow was modeled by the SST  $k-\omega$  turbulent model. The results in daylight demonstrated that energy efficiency increases steadily by 11:30 a.m., and then, starts to drop gradually due to more irradiations at noon. It was observed that applying the turbulator to the studied PTSC has a significant influence on the enhancement of energy efficiency. Adding the nanoparticles augmented the average Nusselt number inside the solar collector in various studied Reynolds numbers. It was also found that the increase in volume concentrations of nanoparticles enhances heat transfer regularly.

**Keywords:** parabolic trough solar collector (PTSC); hybrid nanofluid; mesoporous silica modified with copper; energy efficiency; exergy efficiency

## 1. Introduction

Solar thermal systems have been known as a significant and reliable renewable energy sources for providing clean energy and an important alternative to fossil fuel energy sources. A parabolic trough solar collector (PTSC) is an innovative and effective concentrating solar system that can be used for a variety of industrial and domestic applications. In the last decade, different concepts and ways were introduced and tested to improve the efficiency of PTSC. Among the applied methods, two advanced techniques which showed promising results were employing turbulators and nanofluids for increasing the thermal characteristics of PTSCs. However, pressure drop plays a key drawback in the cited methods, which can affect their applications. Therefore, it is crucial that a thermal–hydraulic approach

should be considered to investigate the nanofluid-based solar collectors. Furthermore, energy and exergy analysis can play a significant role in designing PTSCs efficiently.

Yuehong et al. [1] analyzed the performance of solar air conditioning systems based on an independent-developed solar collector. Their obtained results illustrated that a solar air conditioning system with a three-phase (3P) accumulator can supply building cooling steadily and is satisfactory economically. The mean efficiency and the energy fraction of the studied solar collector in their work were about 68 and 83 percent, respectively. Chen et al. [2] investigated the performance of a three-dimensional heat exchanger with metal-foam baffle numerically with the purpose of recovering the waste heat. They showed that metal-foam baffle heat exchangers have a better performance compared to conventional heat exchangers. Zheng et al. [3] studied plate heat exchangers' operation behavior and their effects on organic Rankine cycle characteristics experimentally and numerically. They found that the heat transfer area affects the operation of the heat exchangers and the organic Rankine cycle systems substantially. Saleem et al. [4] analyzed thermal characteristics of single-phase fluid flow in a small-scale fin-and-tube refrigerant-to-air heat exchanger experimentally. Ishaque et al. [5] investigated three-dimensional heat exchanger configurations' influences on heat pump systems' seasonal characteristics numerically. They demonstrated that smaller refrigerant circuits at the heat exchanger upper sides lead to higher fluid flow velocity, and consequently, enhance the efficiency of the heat exchanger. Abu-Hamdeh et al. [6] assessed the effects of thermal-hydraulic characteristics in turbulent fluid flow and heat transfer in sector-by-sector helically-coiled tube heat exchangers. They validated their numerical results with previously published empirical data. Tuyen et al. [7] applied a one-dimensional model to optimize the thermal and hydraulic performances of R410A refrigerator fluid flow in a liquid-to-suction triple-tube heat exchanger. They showed that the introduced heat exchanger has higher heat transfer and lower pressure drop than the conventional ones. Ren et al. [8] studied the heat transfer characteristics of capillary heat exchange in a metro running tunnel. Having higher thermal efficiency in the heat exchanger, they proved that the system pipe length capillary heat exchanger must be reserved within four meters and each set capillary heat exchanger should be operated separately. However, it was found that the velocity air flow during summer and winter has different influences on the surrounding rock recovery. Ghorbani et al. [9] used PTSCs in a hybrid renewable energy system for fresh water and power production. Due to supply of the input heat, a combined structure of PTSCs, and for condenser cooling, supplement of organic Rankin cycle, the regasification operations were employed. Exergy analysis was considered to evaluate the quality of the integrated structure. They reported that the highest exergy is obtained in the heat exchangers and collectors by 50.23% and 38.18%. Wang et al. [10] studied operation of steam generation system in the presence of a solar collector under cloudy conditions to optimize the system. They reported that the exergy efficiency of plant parasitic power consumption and the thermal energy storage system could change under cloudy conditions. However, the steam generation system operating condition optimization has not been considered properly. García et al. [11] modeled and simulated a solar collector and analyzed its thermal efficiency. They employed an iterative calculation sequence in Python software. They validated their models and results with previous studies and showed a good agreement with them. Wei et al. [12] developed a simplified dynamic model of an integrated solar collector to model and modify present numerical procedures. The validations of steady-state and two dynamic cases showed the accuracy of the applied numerical approach. They also demonstrated the combined procedure may be applied to test system controllers, the solar collector, and other different zones connected to the solar collector. Xu et al. [13] analyzed the effects of thermal and optical factors on the transient performance of a solar collector. The comparison between their numerical results and experimental data illustrated a reliable and sensible coincidence. They determined the temperature distributions on the absorber tube and glass cover.

Sadripour [14] studied atmospheric-aerosol/carbon-black nanofluid flow within a solar air heater located in Shiraz, Iran. Rashidi et al. [15] simulated the natural convection heat transfer and entropy generation in a three-dimensional vertical cylinder filled with nanofluid. Sadripour [16]

investigated flow characteristics and heat transfer enhancement of a corrugated duct using nanofluid. Mahian et al. [17,18] reported and analyzed recent fundamentals, theories, applications and advances in modeling and simulation of nanofluid flows. Sadripour [19] analyzed first and second laws efficiencies and optimization of a solar absorber, using insulator mixers and MWCNTs nanoparticles. Al-Rashed et al. [20] conducted a numerical research into effects of movable-baffles on thermal efficiency and entropy generation of a three-dimensional cavity saturated filled with CNT-nanofluid. Kolsi et al. [21] studied buoyancy-induced flow and entropy generation in a three-dimensional cavity equipped with adiabatic diamond-shape turbulators filled with nanofluid. Two different viewpoints about using aerosol-carbon nanofluid in corrugated solar collectors—thermal–hydraulic performance and heating performance—were evaluated by Sadripour et al. [22]. Rashidi et al. [23] investigated inserts and nanofluid combination for thermal improvement of heat exchangers. He et al. [24] studied numerically the effect of using a novel compound nucleating agent calcium sulfate whisker/ $\beta$ -nucleating agent dicyclohexyl-terephthalamide on crystallization and melting behavior of isotactic polypropylene. Rashidi et al. [25] reviewed different nanofluids' applications in condensing and evaporating systems. Abbasian Arani et al. [26] analyzed the effect of nanoparticle shape on thermal–hydraulic performance of boehmite alumina nanofluids in a sinusoidal wavy mini-channel with phase shift and variable wavelength. Sadripour et al. [27] performed a numerical study for a full convection–conduction–radiation coupling in a cavity equipped with corrugated heat source. Moghaddaszadeh et al. [28] examined the potential of using gear ring shape turbulators in a three-dimensional heat exchanger tube in view of entropy generation.

The literature review clarifies that there is a lack of studies analyzing the effects of turbulators on energy and exergy in a PTSC filled with nanoparticles of Cu/SBA-15. The main aim of present work is to simulate the corrugated PTSC equipped with a turbulator and filled with nanofluid using ANSYS Fluent software, and also investigate the effects of different Reynolds numbers, sunny hours and nanoparticles parameters on thermal and hydraulic characteristics, energy efficiency and exergy efficiency of the studied collector.

## 2. Methodology

### 2.1. Physical Model and Governing Equations

Figure 1 illustrates schematic diagram of the simulated three-dimensional (3D) corrugated PTSC. Figure 2 shows geometrical dimensions of the studied geometry. The absorber tube is made of stainless steel 304 with 2mm thickness, which absorbs the solar energy, and the thickness of the glass cover is 2.5 mm. The turbulator is made of stainless steel 304. The both turbulator and glass cover have also energy absorption. A wide range of Reynolds numbers in the turbulent regime are investigated between  $Re = 3200$  and  $7500$  to the study effects of flow velocity on energy and exergy efficiencies. The solar energy data for a certain position during different sunny hours are studied to consider the collector energy operation at different times. For all studied models, the inlet nanofluid temperature is  $T_{in} = 38$  °C and the solar energy irradiance is adopted based on Figure 3. A Newtonian hybrid nanofluid based on the carrier fluid of water and nanoparticles of mesoporous silica modified with copper (Cu/SBA-15) are applied in present study. To satisfy the Newtonian condition of the employed nanofluid, the volume concentration of the nanoparticle is considered between 0.019% and 0.075%.

The thermophysical properties of nanofluids are calculated as follows [29]:

$$\rho_{hmf} = (1 - \phi_{SBA}) \left[ (1 - \phi_{Cu}) \rho_{bf} + \phi_{Cu} \rho_{np,Cu} \right] + \phi_{SBA} \rho_{np,SBA} \quad (1)$$

$$(\rho c_p)_{hmf} = (1 - \phi_{SBA}) \left[ (1 - \phi_{Cu}) (\rho c_p)_{bf} + \phi_{Cu} (\rho c_p)_{np,Cu} \right] + \phi_{SBA} (\rho c_p)_{np,SBA} \quad (2)$$

The effective density  $\rho_{hmf}$  and specific heat  $c_{p,hmf}$  of the nanofluid at each section-temperature ( $T_m$ ) are determined using the Equations (1) and (2), where  $\phi_{Cu}$  and  $\phi_{SBA}$  are the volume concentration

and density of Cu and SBA-15 nanoparticles, respectively.  $\rho_{bf}$  and  $\rho_{np}$  are the density of water and nanoparticles, respectively.

The effective thermal conductivity and dynamic viscosity of nanofluid are determined by the following equation:

$$\frac{k_{nf}}{k_{bf}} = a_1 T^{a_2} + a_3 \phi_{np}^{a_4} + a_5 (T\phi)^{a_6} - a_7 \quad (3)$$

$$a_1 = 15.850768731, \quad a_2 = 0.0094414758866, \quad a_3 = 1.5096876947, \quad a_4 = 0.12126304132, \\ a_5 = 0.042232628685, \quad a_6 = -1.3077619099, \quad a_7 = 16.312735992 \quad (4)$$

$$\mu_{mf} = \frac{\mu_{bf}}{(1 - \phi_{Cu})^{2.5} (1 - \phi_{SBA})^{2.5}} \quad (5)$$

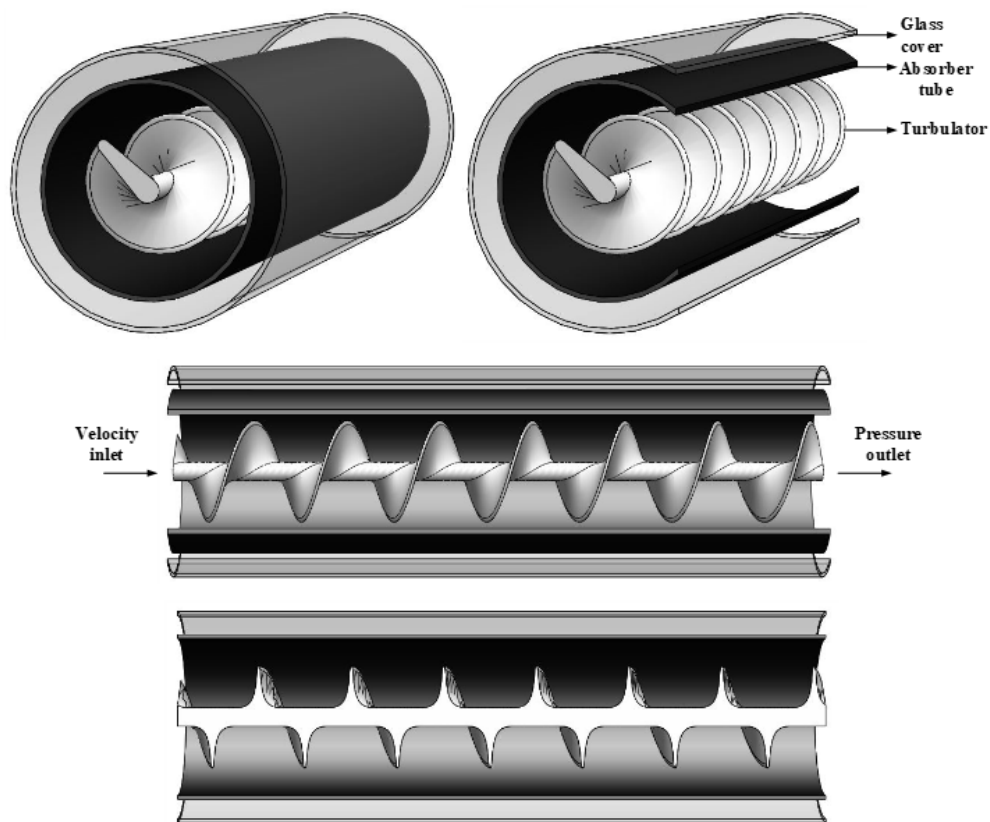


**Figure 1.** Schematic diagrams of the studied capsule heat exchanger and its geometrical parameters.

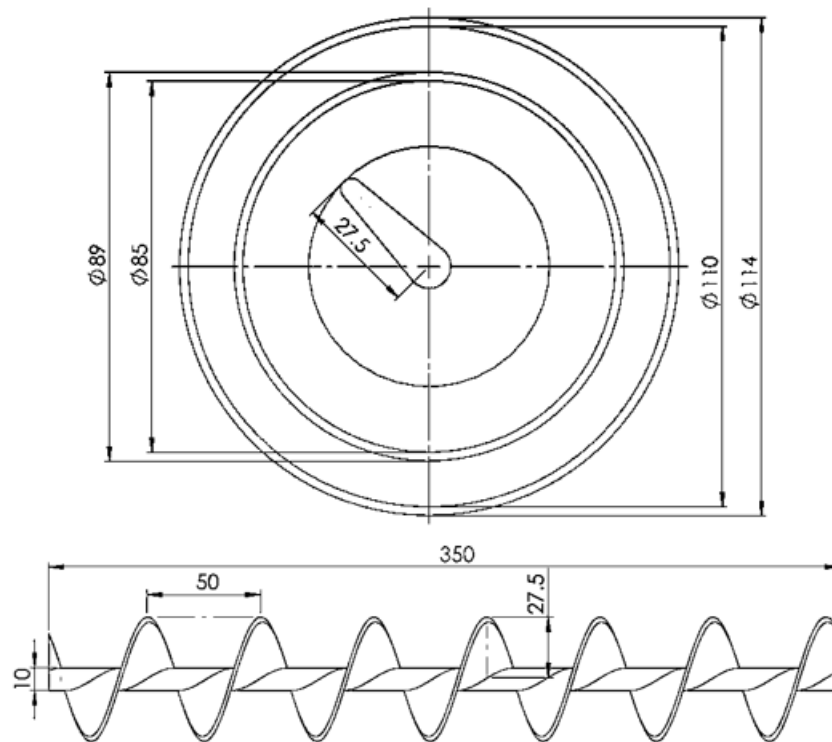


Figure 2. Geometrical dimensions of studied geometry.

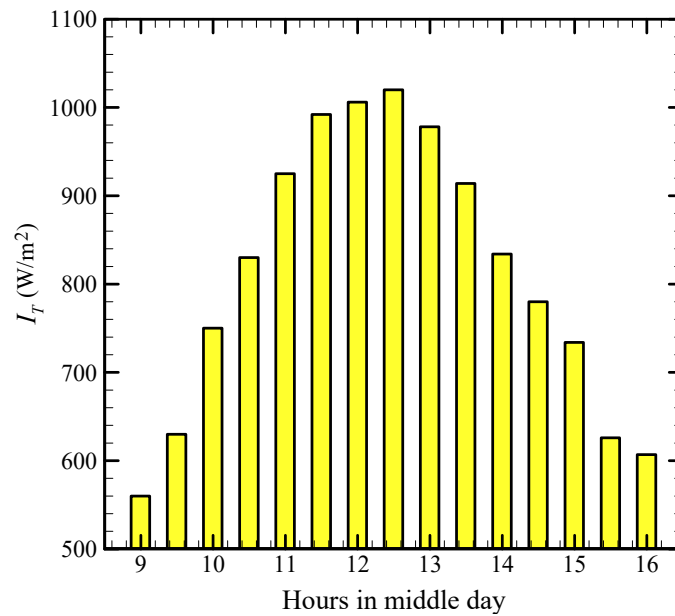


Figure 3. Solar irradiations during a day [29].

A three-dimensional computational fluid dynamic procedure is established to study the turbulent nanofluid flow and heat transfer performances in the studied PTSC. The three-dimensional governing equations are as follows [30–32]:

Continuity equation:

$$\frac{\partial}{\partial x_i}(\rho u_i) = 0 \tag{6}$$

Momentum equation:

$$\frac{\partial}{\partial x_i}(\rho u_i u_j) = -\frac{\partial p}{\partial x_i} + \frac{\partial \tau_{ij}}{\partial x_j} + \rho g_i \quad (7)$$

$$\tau_{ij} = \frac{\mu^* \partial u_i}{\partial x_j} \quad (8)$$

$$\mu^* = \mu + \mu_t \quad (9)$$

Energy equation:

$$\frac{\partial}{\partial x_i}(\rho c_p u_i T) = \frac{\partial}{\partial x_i} \left( \frac{\lambda^* \partial T}{\partial x_i} \right) \quad (10)$$

$$\lambda^* = \lambda + \lambda_t \quad (11)$$

$$\lambda_t = \frac{c_p \mu_t}{\sigma_t} \quad (12)$$

The RANS equations with the shear-stress (SST)  $k$ - $\omega$  turbulent model are employed for modeling the turbulent regime. The mathematical model can be described as [33]:

$$\frac{\partial}{\partial x_i}(\rho u_i k) = \frac{\partial}{\partial x_i} \left[ \left( \mu + \frac{\mu_t}{\sigma_k} \right) \frac{\partial k}{\partial x_i} \right] + G_k - Y_k \quad (13)$$

$$\frac{\partial}{\partial x_i}(\rho u_i \omega) = \frac{\partial}{\partial x_i} \left[ \left( \mu + \frac{\mu_t}{\sigma_\omega} \right) \frac{\partial \omega}{\partial x_i} \right] + G_\omega - Y_\omega + D_\omega \quad (14)$$

$$\mu_t = \frac{\rho k}{\omega} \frac{1}{\max\left\{ \frac{1}{\alpha^*}, \frac{\Omega F_2}{a_1 \omega} \right\}} \quad (15)$$

$$\Omega = \sqrt{2\Omega_{ij}\Omega_{ij}} \quad (16)$$

It is reported that the SST  $k$ - $\omega$  turbulent model [33] can be an effective tool for studying the strong acceleration and large normal strain in a fluid flow and adverse pressure gradients, which can be observed in a nanofluid flow near solid boundaries. The specific dissipation rate ( $\omega$ ) and the turbulence kinetic energy ( $k$ ) in the SST  $k$ - $\omega$  are defined as [33]:

$$\Omega_{ij} = \frac{1}{2} \left( \frac{\partial u_i}{\partial x_j} - \frac{\partial u_j}{\partial x_i} \right) \quad (17)$$

$$\sigma_k = \frac{1}{\frac{F_1}{\sigma_{k,1}} + \frac{1-F_1}{\sigma_{k,2}}} \quad (18)$$

$$\sigma_\omega = \frac{1}{\frac{F_1}{\sigma_{\omega,1}} + \frac{1-F_1}{\sigma_{\omega,2}}} \quad (19)$$

$$F_1 = \tanh(\Phi_1^4) \quad (20)$$

$$F_2 = \tanh(\Phi_2^2) \quad (21)$$

$$\Phi_1 = \min \left\{ \max \left\{ \frac{\sqrt{k}}{0.09\omega y}, \frac{500\mu}{\rho y^2 \omega} \right\}, \frac{4\rho k}{\sigma_{\omega,2} D_\omega^+ y^2} \right\} \quad (22)$$

$$\Phi_2 = \max \left\{ \frac{2\sqrt{k}}{0.09\omega y}, \frac{500\mu}{\rho y^2 \omega} \right\} \quad (23)$$

$$D_\omega^+ = \max \left\{ \frac{2\rho}{\omega \rho_{\omega,2}} \frac{\partial k}{\partial x_i} \frac{\partial \omega}{\partial x_i}, 10^{-20} \right\} \quad (24)$$

$$\alpha^* = \alpha_\infty^* \left( \frac{\alpha_0^* + \frac{Re_t}{R_k}}{1 + \frac{Re_t}{R_k}} \right), \quad \alpha_0^* = \frac{\beta_i}{3}, \quad Re_t = \frac{\rho k}{\mu \omega}, \quad \beta_i = F_1 \beta_{i,1} + (1 - F_1) \beta_{i,2} \quad (25)$$

$$G_k = \tau_{t,ij} \frac{\partial u_i}{\partial x_j}, \quad \tau_{t,ij} = \mu_t \left( \frac{\partial u_i}{\partial x_j} + \frac{\partial u_j}{\partial x_i} \right) - \frac{2}{3} \rho k \delta_{ij} \quad (26)$$

$$Y_k = \rho \beta^* k \omega, \quad G_\omega = \frac{\rho \alpha}{\mu_t} G_k, \quad Y_\infty = \rho \beta_i \omega^2 \quad (27)$$

$$\alpha = \frac{\alpha_\infty}{\alpha^*} = \left( \frac{\alpha_0^* + \frac{Re_t}{R_k}}{1 + \frac{Re_t}{R_k}} \right), \quad \alpha_\infty = F_1 \alpha_{\infty,1} + (1 - F_1) \alpha_{\infty,2} \quad (28)$$

$$\alpha_{\infty,1} = \frac{\beta_{i,1}}{\beta_\infty^*} - \frac{\kappa^2}{\sigma_{\omega,1} \sqrt{\beta_\infty^*}}, \quad \alpha_{\infty,2} = \frac{\beta_{i,2}}{\beta_\infty^*} - \frac{\kappa^2}{\sigma_{\omega,2} \sqrt{\beta_\infty^*}} \quad (29)$$

where  $\Omega_{ij}$  is the mean rate-of-rotation tensor and  $F_1$  and  $F_2$  are the blending functions.  $D_\omega^+$  is the cross-diffusion term, positive portion [33]. The constant values are cited in Table 1. The studied equations were solved until the grid control volume maximum residual became less than  $10^{-6}$ .

**Table 1.** Values of constants in the SST  $k$ - $\omega$  turbulence model [33].

$\sigma_t$	$\alpha_{k,1}$	$\alpha_{k,2}$	$\alpha_{\omega,1}$	$\alpha_{\omega,2}$	$a_1$	$\beta_{i,1}$	$\beta_{i,2}$	$\beta_\infty^*$	$\kappa$	$R_k$
0.85	1.176	1.000	2.000	1.168	0.31	0.0750	0.0828	0.0900	0.41	6

To compare and analyze the fluid flow characteristics and heat transfer of various geometries in the studied collector, some definitions are given as follows [30,31]:

The Reynolds number is defined as:

$$Re = \frac{\rho u_m D_h}{\mu} \quad (30)$$

where  $u_m$  is the fluid or nanofluid average velocity over the cross section. The average Nusselt number is expressed as:

$$Nu_{av} = \frac{h_{bf} D_h}{k_{bf}} \quad (31)$$

where  $h_{bf}$  and  $k_{bf}$  are average heat transfer coefficient and the thermal conductivity of base fluid, respectively. The pressure drop between inlet and outlet of test section is defined as:

$$\Delta P = P_{av,inlet} - P_{av,outlet} \quad (32)$$

The friction factor coefficient for fully developed flow is defined as:

$$f = \frac{2}{\left(\frac{L_2}{D_h}\right)} \frac{\Delta P}{\rho_{nmf} u_m^2} \quad (33)$$

In addition, the absorbed energy is calculated using the following equation:

$$Q_{u,c} = A_c [S - U_L (T_{pm} - T_a)] \quad (34)$$

The energy and exergy efficiencies are calculated as follows:

$$\eta = \frac{\dot{m}_f \cdot c_p (T_{out} - T_{in}) - P}{I_T A_c} \quad (35)$$

$$\varepsilon = \frac{\dot{E}_{out,f} - \dot{E}_{in,f}}{I_T A_C \left(1 - \frac{T_a}{T_s}\right)} \quad (36)$$

## 2.2. Validation

Grid independence tests were performed for different grid sizes and Reynolds numbers in the studied parameters of  $\phi = 0.075\%$ ,  $Re = 7400$  and the time of 12:30 p.m. Table 2 demonstrated that the grid size with 2,018,210 nodes results in a satisfactory agreement between the computational time and the accuracy of results with the maximum error of 2% (see Figure 4a). Present computational fluid dynamics (CFD) results were validated with the experimental data of Wang et al. [34] and depicted in Figure 4b at  $\phi = 0.075\%$ ,  $Re = 7400$  and 12:30 p.m. It shows that there is a good agreement (with maximum 9.68% error) between the results of Wang et al. [34] and the present study.

**Table 2.** Grid independence test in terms of outlet temperature increase in the parabolic trough solar collector using nanofluid at  $\phi = 0.075\%$ ,  $Re = 7400$  and the time of 12:30 p.m.

Grid Number	Nodes	$\Delta T_{out}$ (°C)	Error (%)
1	526,928	15.8372	70.17
2	892,267	27.1202	36.52
3	1,276,128	36.7829	11.87
4	1,728,919	40.5289	2.92
5	1,917,010	41.1301	1.47
6	2,018,210	42.1801	0.02
7	2,289,192	42.1824	-

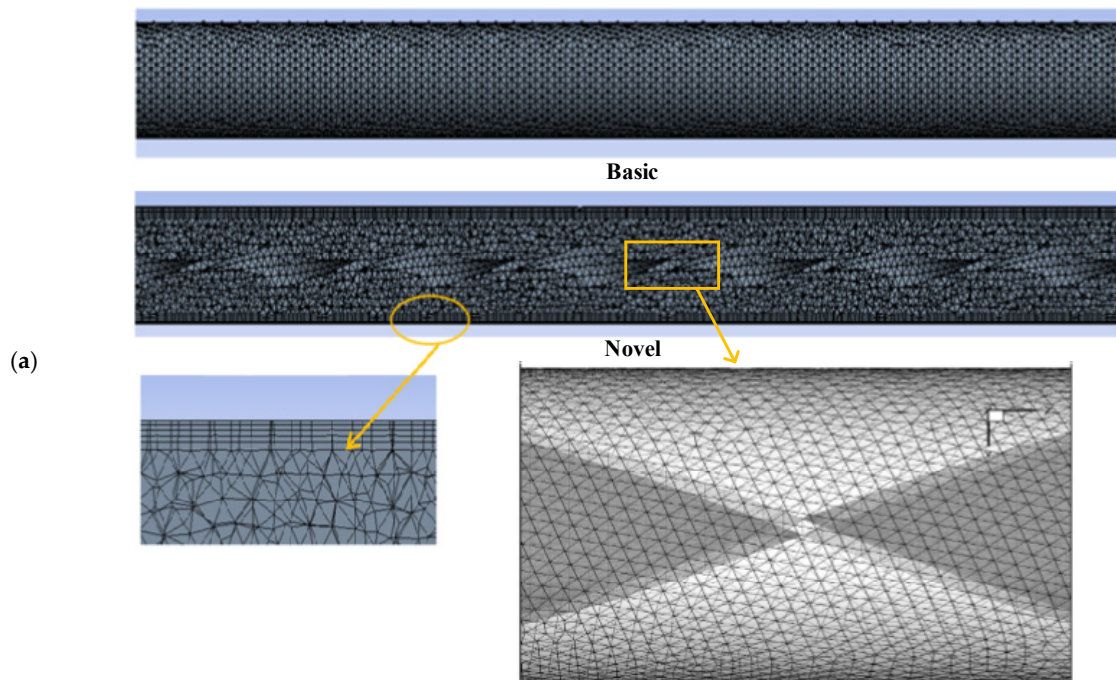


**Figure 4.** Cont.



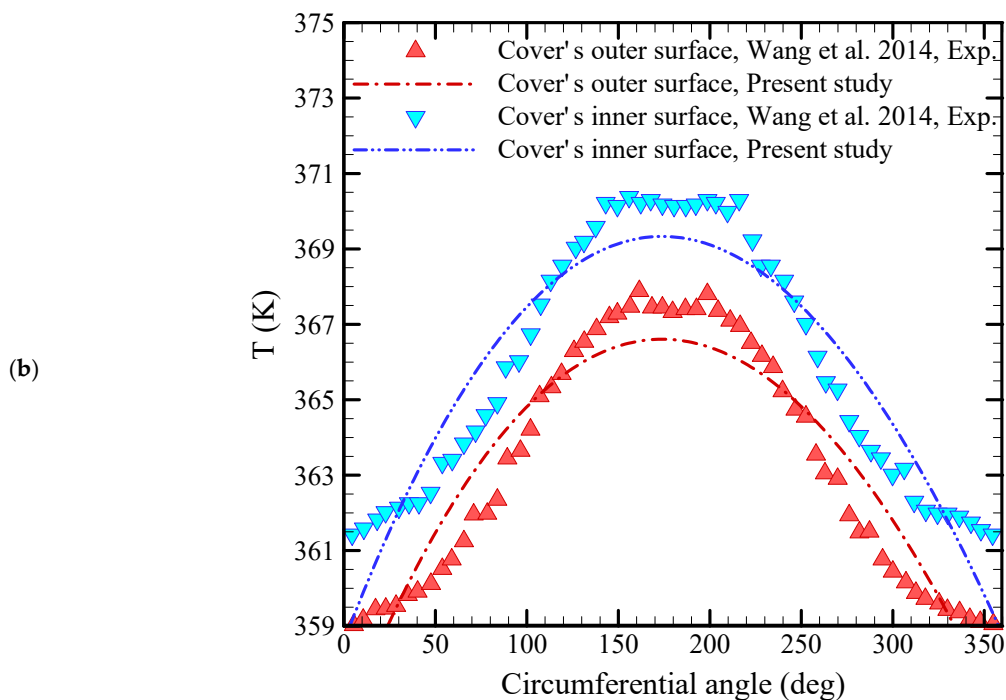
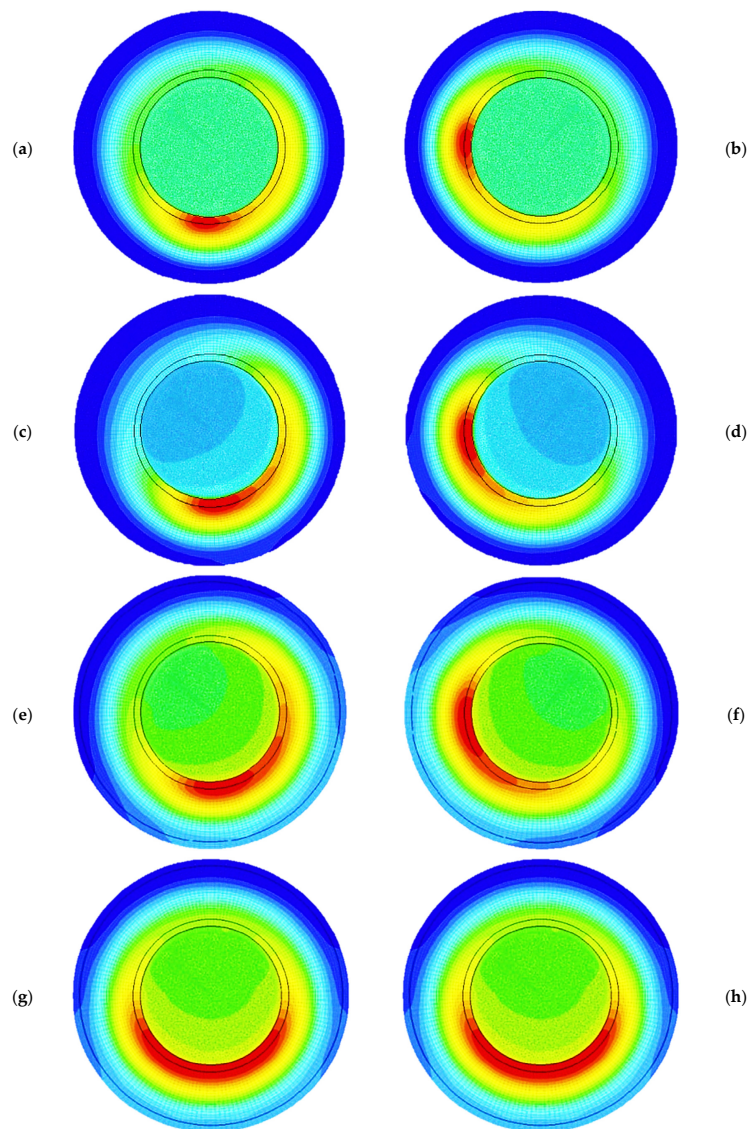


**Figure 4.** (a) Grid mesh. (b) Code validation among present work results and experimental data of Wang et al. [34].

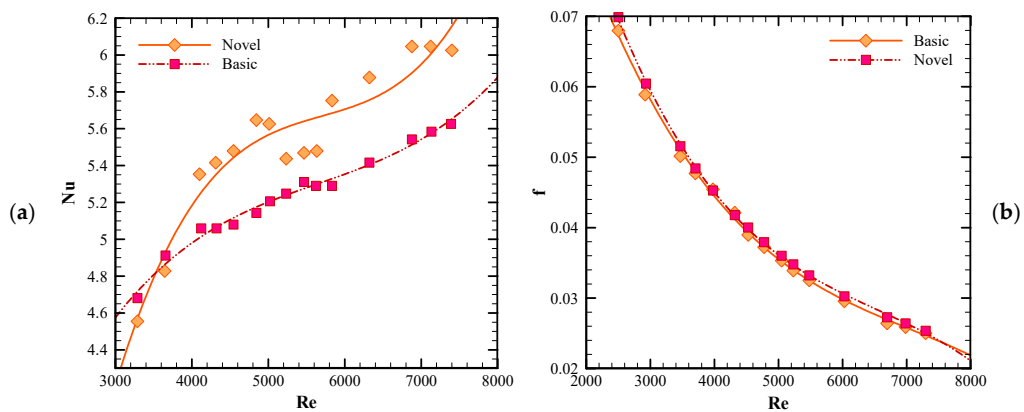
### 3. Results and Discussion

Figure 5 demonstrates temperature contours for a PTSC equipped with a turbulator and filled with a nanofluid at  $\phi = 0.075\%$ ,  $Re = 7400$  and the time of 12:30 p.m. in different positions of the collector (a)  $x = 55$  mm, (b)  $x = 80$  mm, (c)  $x = 105$  mm, (d)  $x = 130$  mm, (e)  $x = 155$  mm, (f)  $x = 180$  mm, (g)  $x = 205$  mm, and (h)  $x = 255$  mm. It is clear that the usage of the turbulator has a significant influence on heat transfer and energy absorption. It is also observed that the energy concentration in the tube is located on the position of helix.

Figure 6 shows variation of average Nusselt number and friction factor versus different Reynolds numbers for the PTSC system without a turbulator (basic) and with the turbulator (novel) in the presence of the nanofluid at  $\phi = 0.019\%$  and time 12:30 p.m. Figure 6a illustrates that the average Nusselt number increases steadily by the rise of the Reynolds number in the two studied cases. It also depicts that the usage of turbulator has a sharp influence on heat transfer inside the solar collector. Furthermore, it is evident that at low Reynolds numbers ( $Re < 3500$ ), the average Nusselt number in the novel solar collector is lower than the basic one. Yet, at Reynolds numbers of  $Re > 3500$ , the average Nusselt number in the novel solar collector is more than the basic system. Figure 6b reveals that the average friction factor reduces by an increase in Reynolds numbers gradually, and the presence of turbulator increases the pressure drop and friction factor inside the solar collector marginally. However, it is clear that the average friction factor in novel and basic solar collectors follows the same pattern. In fact, turbulators generate vortexes in the channel which destroy the laminar sub-layers and enhance the mixing rate. Consequently, turbulators augment the heat transfer coefficient in the channel, and therefore, increase the value of the average Nusselt number. The average Nusselt number rises by the increase in the Reynolds number since it strengthens flow velocities and vortex generation in the channel, and consequently, enhances the heat transfer coefficient and average Nusselt number.



**Figure 5.** Temperature contours for PTSC equipped with a turbulator and filled with nanofluid at  $\phi = 0.075\%$ ,  $Re = 7400$  and time 12:30 through the collector: (a)  $x = 55$  mm, (b)  $x = 80$  mm, (c)  $x = 105$  mm, (d)  $x = 130$  mm, (e)  $x = 155$  mm, (f)  $x = 180$  mm, (g)  $x = 205$  mm, and (h)  $x = 255$  mm.



**Figure 6.** Variation of average (a) Nusselt number and (b) friction factor for a basic system without a turbulator and novel PTSC equipped with a turbulator and filled with nanofluid at  $\phi = 0.019\%$  and time 12:30 versus different Reynolds numbers.

Figure 7 illustrates the variation of heat loss for basic and novel systems at  $\phi = 0.019\%$  and  $Re = 5000$  versus different times of a day. It shows that the heat loss in a novel system is lower than the basic system at all hours. The turbulator has a substantial influence on energy loss ratio inside the solar collector, but the energy loss ratio is different for various times. Figure 8 shows the variation of absorber plate temperature for basic and novel systems at  $\phi = 0.019\%$  and  $Re = 5000$  versus different times of a day. Furthermore, the absorber mean temperature increases by the rise in times in sunny hours, because of presence of close cycle in the studied solar system. It is also notable that the absorber mean temperature in the novel solar collector is higher than the basic system. Figure 9 illustrates the variation of outlet temperature for basic and novel systems at  $\phi = 0.019\%$  and  $Re = 5000$  versus different times of day. It demonstrates that during all studied sunny hours, the outlet temperature enhances by the increase in hours because of the close cycle in the solar system. It clarifies that the outlet temperature in the novel solar collector is more than the basic system. In addition, it shows that thermal and hydraulic performances of the novel and basic systems are different and the novel system has higher energy (heat transfer) characteristics than the basic one, while their hydraulic characteristics are nearly the same, because of the special shape of the turbulator. The energy and exergy efficiencies of the collectors are displayed in Figure 10 at  $\phi = 0.019\%$  and  $Re = 5000$  for different times. It is seen that the energy efficiency augments gradually and reaches in its peak at 11.30 a.m., and then, drops steadily due to more irradiations at noon. Furthermore, it is found that the energy efficiency in the novel solar collector is stronger than the energy efficiency in the basic one. Figure 11 illustrates variation of exergy efficiency for the basic system without a turbulator and the novel PTSC equipped with a turbulator and filled with nanofluid at  $\phi = 0.019\%$  and  $Re = 5000$  for different times of a day.

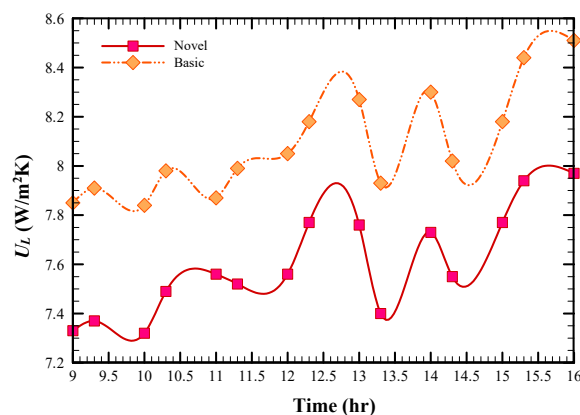


**Figure 7.** Variation of heat loss for the basic system without a turbulator and novel PTSC equipped with a turbulator and filled with nanofluid at  $\phi = 0.019\%$  and  $Re = 5000$  versus different times of day.

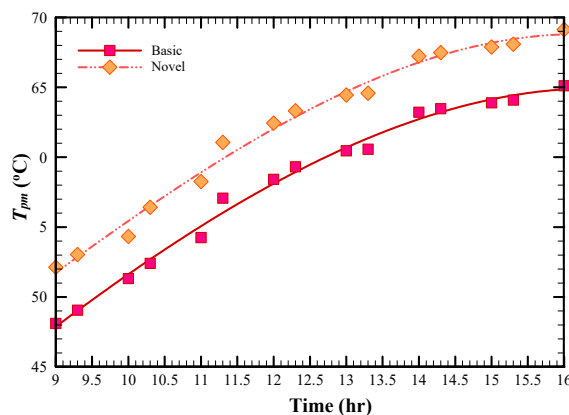


**Figure 8.** Variation of absorber plate temperature for a basic system without a turbulator and novel PTSC equipped with a turbulator and filled with nanofluid at  $\phi = 0.019\%$  and  $Re = 5000$  versus different times of day.

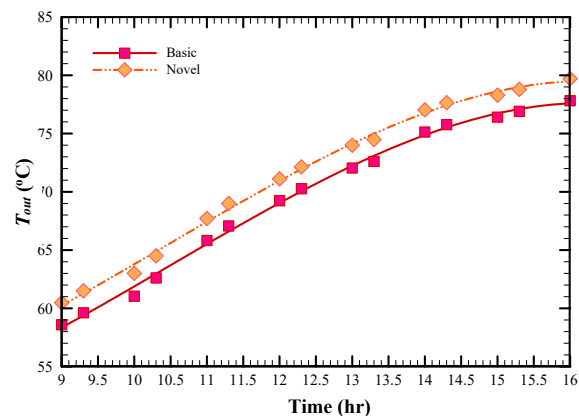


**Figure 9.** Variation of outlet temperature for a basic system without a turbulator and novel PTSC equipped with a turbulator and filled with nanofluid at  $\phi = 0.019\%$  and  $Re = 5000$  versus different times of day.

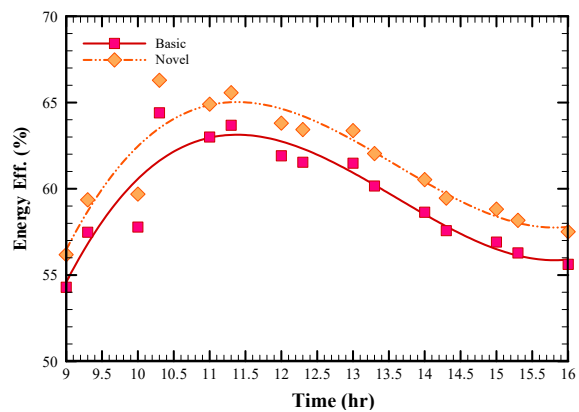


**Figure 10.** Variation of energy efficiency for a basic system without a turbulator and novel PTSC equipped with a turbulator and filled with nanofluid at  $\phi = 0.019\%$  and  $Re = 5000$  versus different times of day.

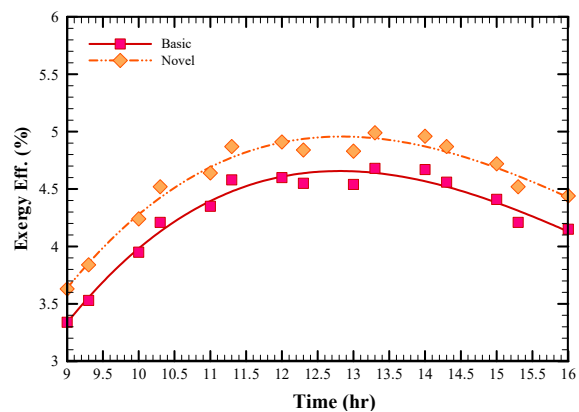


**Figure 11.** Variation of exergy efficiency for a basic system without a turbulator and novel PTSC equipped with a turbulator and filled with nanofluid at  $\phi = 0.019\%$  and  $Re = 5000$  versus different times of day.

It is obvious that the exergy efficiency increases until 13:00, and then, reduces gradually. It also shows that the exergy efficiency in the novel solar collector is bigger than the exergy efficiency of the basic one. Figure 12 presents the variation of absorbed energy for a basic system without a turbulator and a novel one at  $\phi = 0.019\%$  and  $Re = 5000$  at different times of a day. It is observed that the absorbed

energy value increases significantly until 12:30, and then, falls considerably. It also demonstrates that the presence of the turbulator does not affect the energy absorption noticeably and the energy absorption in novel and basic solar collectors follow the same trend. However, the energy absorption in the novel solar collector is marginally higher than the basic system.

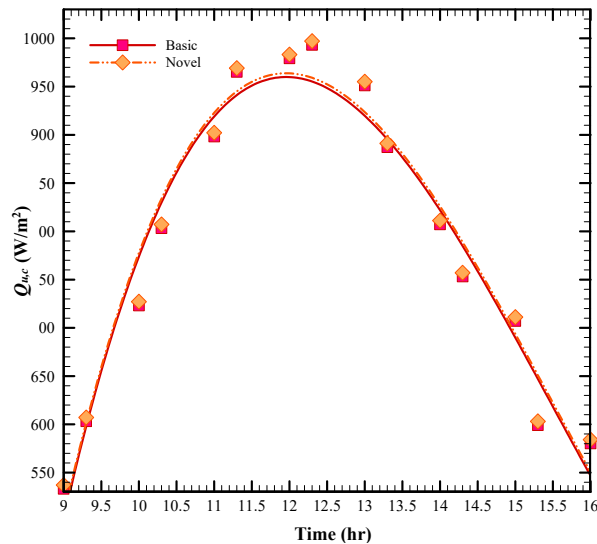


**Figure 12.** Variation of absorbed energy for a basic system without a turbulator and novel PTSC equipped with a turbulator and filled with nanofluid at  $\phi = 0.019\%$  and  $Re = 5000$  versus different times of day.

Figure 13 demonstrates the variation of average Nusselt number for a novel PTSC equipped with a turbulator and filled with nanofluid in different volume fractions of nanoparticles and Reynolds numbers at time 12:30. The average Nusselt number value is increased by the enhancement of Reynolds numbers in various volume fractions of nanoparticles. It also indicates that the novel solar collector with 0.075% volume concentration has the highest Nusselt number values among all studied models, which is followed by the volume concentrations of 0.050%, 0.040% and 0.019%, respectively.

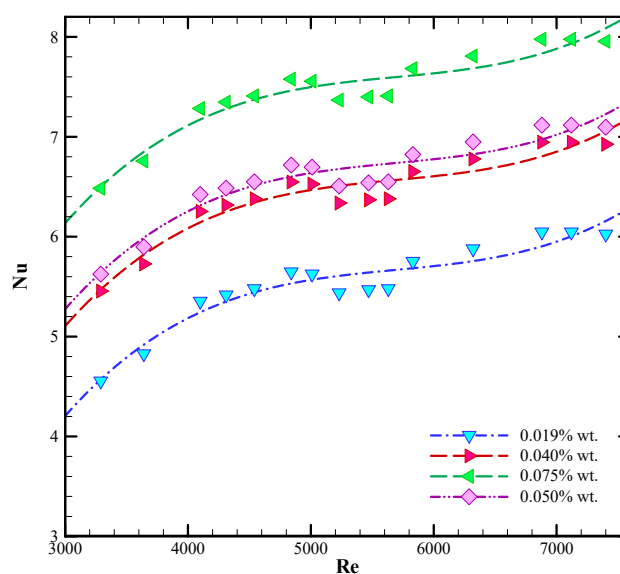


**Figure 13.** Variation of average Nusselt number for novel PTSC equipped with a turbulator and filled with nanofluid in different volume fractions of nanoparticles versus different Reynolds numbers at time 12:30.

#### 4. Conclusions

Present numerical study investigates energy and exergy analysis of using turbulator in a PTSC filled with mesoporous silica modified with copper nanoparticles hybrid nanofluid. The main aim of present work is to simulate the corrugated PTSC equipped with a turbulator and filled with nanofluid using the ANSYS Fluent software. The effects of different Reynolds numbers, sunny hours and nanoparticles parameters on thermal and hydraulic characteristics, energy efficiency and exergy efficiency of the studied collector were evaluated and reported. The three-dimensional absorber tube is made of stainless steel 304 with 2 mm thickness, which absorbs the solar energy and the glass cover has 2.5 mm thickness. The three-dimensional turbulator is also made of stainless steel 304. Both the turbulator and glass cover also have energy absorption. Sixteen different Reynolds numbers are studied in the range of  $3200 < Re < 7500$  to assess the effects of flow velocity on energy and exergy efficiencies as well as the value of absorbed energy in the collector. The solar energy data in a certain position for different times were studied to consider the collector energy operation during a day. To generate the Newtonian nanofluid, the Cu/SBA-15 was added to the water in the volume concentration of 0.019% to 0.075%. The SST  $k-\omega$  turbulent model was applied for this study since it was reported that this model is a promising tool in studying nanofluid flow in complex geometries. Results showed that the exergy efficiency during the daylight increases steadily until 13:00, and then, dropped gradually. It was found that applying the turbulator enhances the exergy efficiency in PTSC considerably. It was also observed absorbed energy value by time increases before 12:30, but declines after this time. It was also noticed that the turbulator does not have a significant influence on energy absorption inside the solar collector. It was revealed that the average Nusselt number is augmented by the rise of the Reynolds number. Moreover, it was demonstrated that the addition of the nanofluid has a substantial effect on average Nusselt number inside the solar collector. The increase in the volume fraction of the nanoparticles enhanced the average Nusselt number, and therefore, the highest average Nusselt number was achieved at the volume concentration of  $\phi = 0.075\%$ .

**Author Contributions:** Main idea, S.R.; simulation, A.S.; formal analysis, S.R. and A.S.; writing—original draft preparation, S.R. and A.S.; writing—review and editing, G.K.; Drafted or provided critical revision of the article, A.S.G. All authors have read and agreed to the published version of the manuscript.

**Funding:** This research received no external funding.

**Conflicts of Interest:** The authors declare no conflict of interest.

#### Nomenclature

##### Symbols

A	Surface area (m <sup>2</sup> )
$c_p$	Specific heat capacity, (J/kgK)
D	Diffusion
D <sub>h</sub>	Hydraulic diameter, (m)
$D_{\omega}^+$	Cross diffusion term positive portion
d	Diameter of nanoparticles (nm)
$F_1$	Blending function 1
$F_2$	Blending function 2
f	Mean predicted friction factor
k	Thermal conductivity, (W/mK)
M	Molar mass
N	Avogadro number
Pr	Prandtl number
p	Pressure, (Pa)
Q	Heat flux (W)
$q''$	Specific heat flux (W/m <sup>2</sup> )
Re	Reynolds number
T	Temperature (K)

u	Velocity
$V_m$	Velocity
Greek Symbols	
$\alpha$	Thermal diffusion
$\mu$	Dynamic viscosity, (Ns/m <sup>2</sup> )
$\rho$	Density, (Kg/m <sup>3</sup> )
$\varphi$	Nanoparticles volume fraction
$\emptyset$	Geometrical diameter (m)
$\Omega_{ij}$	Mean rate-of-rotation tensor
Subscriptions	
B	Brownian
bf	Base fluid
cro	Crude oil
nf	Nanofluid
np	Nanoparticle

## References

- Bi, Y.; Qin, L.; Guo, J.; Li, H.; Zang, G. Performance analysis of solar air conditioning system based on the independent-developed solar parabolic trough collector. *Energy* **2020**, *196*, 117075. [[CrossRef](#)]
- Chen, T.; Tian, H.; Tian, H.; Zhao, T.; Zhang, H.; Zhang, Z. Performance evaluation of metal-foam baffle exhaust heat exchanger for waste heat recovery. *Appl. Energy* **2020**, *266*, 114875. [[CrossRef](#)]
- Zheng, X.; Luo, X.; Luo, J.; Chen, J.; Liang, Y.; Yang, Z.; Chen, Y.; Wang, H. Experimental investigation of operation behavior of plate heat exchangers and their influences on organic Rankine cycle performance. *Energy Convers. Manag.* **2020**, *207*, 112528. [[CrossRef](#)]
- Saleem, S.; Sarfraz, O.; Bradshaw, C.R.; Bach, C.K. Development of novel experimental infrastructure for collection of high-fidelity experimental data for refrigerant to air heat exchangers. *Int. J. Refrig.* **2020**, *114*, 189–200. [[CrossRef](#)]
- Ishaque, S.; Siddiqui, I.H.; Kim, M.-H. Effect of heat exchanger design on seasonal performance of heat pump systems. *Int. J. Heat Mass Transf.* **2020**, *151*, 119404. [[CrossRef](#)]
- Abu-Hamdeh, N.H.; Bantan, R.A.; Tlili, I. Analysis of the thermal and hydraulic performance of the sector-by-sector helically coiled tube heat exchangers as a new type of heat exchangers. *Int. J. Therm. Sci.* **2020**, *150*, 106229. [[CrossRef](#)]
- Tuyen, V.; Van Hap, N.; Phu, N.M. Thermal-hydraulic characteristics and optimization of a liquid-to-suction triple-tube heat exchanger. *Case Stud. Therm. Eng.* **2020**, *19*, 100635. [[CrossRef](#)]
- Ren, M.; Yuan, Y.; Cao, X.; Sun, L.; Jiang, F. Numerical analysis on the thermal performance of capillary heat exchange system in metro running tunnel. *Energy Built Environ.* **2020**, *1*, 207–214. [[CrossRef](#)]
- Ghorbani, B.; Mahyari, K.B.; Mehrpooya, M.; Hamed, M.-H. Introducing a hybrid renewable energy system for production of power and fresh water using parabolic trough solar collectors and LNG cold energy recovery. *Renew. Energy* **2020**, *148*, 1227–1243. [[CrossRef](#)]
- Wang, A.; Liu, J.; Zhang, S.; Liu, M.; Yan, J. Steam generation system operation optimization in parabolic trough concentrating solar power plants under cloudy conditions. *Appl. Energy* **2020**, *265*, 114790. [[CrossRef](#)]
- Quezada-García, S.; Sánchez-Mora, H.; Polo-Labarrios, M.A.; Cázares-Ramírez, R.I. Modeling and simulation to determine the thermal efficiency of a parabolic solar trough collector system. *Case Stud. Therm. Eng.* **2019**, *16*, 100523. [[CrossRef](#)]
- Wei, S.; Liang, X.; Mohsin, T.; Wu, X.; Li, Y. A simplified dynamic model of integrated parabolic trough concentrating solar power plants: Modeling and validation. *Appl. Therm. Eng.* **2020**, *169*, 114982. [[CrossRef](#)]
- Xu, L.; Sun, F.; Ma, L.; Li, X.; Lei, D.; Yuan, G.; Zhu, H.; Zhang, Q.; Xu, E.; Wang, Z.; et al. Analysis of optical and thermal factors' effects on the transient performance of parabolic trough solar collectors. *Sol. Energy* **2019**, *179*, 195–209. [[CrossRef](#)]
- Sadripour, S. 3D numerical analysis of atmospheric-aerosol/carbon-black nanofluid flow within a solar air heater located in Shiraz, Iran. *Int. J. Numer. Methods Heat Fluid Flow* **2019**, *29*, 1378–1402. [[CrossRef](#)]
- Rashidi, I.; Kolsi, L.; Ahmadi, G.; Mahian, O.; Wongwises, S.; Abu-Nada, E. Three-dimensional modelling of natural convection and entropy generation in a vertical cylinder under heterogeneous heat flux using nanofluids. *Int. J. Numer. Methods Heat Fluid Flow* **2019**, *30*, 119–142. [[CrossRef](#)]

16. Sadripour, S. Investigation of flow characteristics and heat transfer enhancement of a corrugated duct using nanofluid. *J. Appl. Mech. Tech. Phys.* **2018**, *59*, 1049–1057. [[CrossRef](#)]
17. Mahian, O.; Kolsi, L.; Amani, M.; Estellé, P.; Ahmadi, G.; Kleinstreuer, C.; Marshall, J.S.; Siavashi, M.; Taylor, R.A.; Niazmand, H.; et al. Recent advances in modeling and simulation of nanofluid flows-Part I: Fundamentals and theory. *Phys. Rep.* **2019**, *790*, 1–48. [[CrossRef](#)]
18. Omid, M.; Lioua, K.; Mohammad, A.; Patrice, E.; Goodarz, A.; Clement, K.; Jeffrey, S.; Marshall, R.A.; Taylor, E.A.-N.; Saman, R.; et al. Recent Advances in Modeling and Simulation of Nanofluid Flows. *Phys. Rep.* **2019**, *791*, 1–59.
19. Sadripour, S. First and second laws analysis and optimization of a solar absorber; using insulator mixers and MWCNTs nanoparticles. *Glob. J. Res. Eng. A Mech. Mech.* **2017**, *17*, 37–48.
20. Al-Rashed, A.A.; Aich, W.; Kolsi, L.; Mahian, O.; Hussein, A.K.; Naceur, B.M. Effects of movable-baffle on heat transfer and entropy generation in a cavity saturated by CNT suspensions: Three-dimensional modeling. *Entropy* **2017**, *19*, 200. [[CrossRef](#)]
21. Kolsi, L.; Mahian, O.; Öztop, H.F.; Aich, W.; Borjini, M.N.; Abu-Hamdeh, N.; Ben Aissia, H. 3D buoyancy-induced flow and entropy generation of nanofluid-filled open cavities having adiabatic diamond shaped obstacles. *Entropy* **2016**, *18*, 232. [[CrossRef](#)]
22. Sadripour, S.; Adibi, M.; Sheikhzadeh, G.A. Two different viewpoints about using aerosol-carbon nanofluid in corrugated solar collectors: Thermal-hydraulic performance and heating performance. *Glob. J. Res. Eng. A Mech. Mech.* **2017**, *17*, 19–36.
23. Rashidi, S.; Eskandarian, M.; Mahian, O.; Poncet, S. Combination of nanofluid and inserts for heat transfer enhancement. *J. Therm. Anal. Calorim.* **2018**, *135*, 437–460. [[CrossRef](#)]
24. He, B.; Lin, X.-F.; Zhang, Y.-F. Effect of a novel compound nucleating agent calcium sulfate whisker/ $\beta$ -nucleating agent dicyclohexyl-terephthalamide on crystallization and melting behavior of isotactic polypropylene. *J. Therm. Anal. Calorim.* **2018**, *132*, 1145–1152. [[CrossRef](#)]
25. Rashidi, S.; Mahian, O.; Languri, E.M. Applications of nanofluids in condensing and evaporating systems. *J. Therm. Anal. Calorim.* **2017**, *131*, 2027–2039. [[CrossRef](#)]
26. Arani, A.A.A.; Sadripour, S.; Kermani, S. Nanoparticle shape effects on thermal-hydraulic performance of boehmite alumina nanofluids in a sinusoidal-wavy mini-channel with phase shift and variable wavelength. *Int. J. Mech. Sci.* **2017**, *128*, 550–563. [[CrossRef](#)]
27. Sadripour, S.; Ghorashi, S.A.; Estajloo, M. Numerical investigation of a cavity equipped with corrugated heat source: A full convection-conduction-radiation coupling. *Am. J. Aerosp. Eng.* **2017**, *4*, 27–37. [[CrossRef](#)]
28. Moghaddaszhadeh, N.; Rashidi, S.; Esfahani, J.A. Potential of gear-ring turbulator in three-dimensional heat exchanger tube from second law of thermodynamic viewpoint. *Int. J. Numer. Methods Heat Fluid Flow* **2019**, *29*, 1526–1543. [[CrossRef](#)]
29. Wang, Y.; Liu, Q.; Lei, J.; Jin, H. A three-dimensional simulation of a parabolic trough solar collector system using molten salt as heat transfer fluid. *Appl. Therm. Eng.* **2014**, *70*, 462–476. [[CrossRef](#)]
30. Sadripour, S.; Chamkha, A.J. The effect of nanoparticle morphology on heat transfer and entropy generation of supported nanofluids in a heat sink solar collector. *Therm. Sci. Eng. Prog.* **2019**, *9*, 266–280. [[CrossRef](#)]
31. Kim, D.; Kwon, Y.; Cho, Y.; Li, C.; Cheong, S.; Hwang, Y.; Lee, J.; Hong, D.; Moon, S. Convective heat transfer characteristics of nanofluids under laminar and turbulent flow conditions. *Curr. Appl. Phys.* **2009**, *9*, e119–e123. [[CrossRef](#)]
32. Yang, Y.-T.; Tang, H.-W.; Zeng, B.-Y.; Wu, C.-H. Numerical simulation and optimization of turbulent nanofluids in a three-dimensional rectangular rib-grooved channel. *Int. Commun. Heat Mass Transf.* **2015**, *66*, 71–79. [[CrossRef](#)]
33. Patankar, S.V. *Numerical Heat Transfer and Fluid Flow*; Taylor & Francis Group: Abingdon-on-Thames, UK, 1980.
34. Tseng, Y.; Ferng, Y.; Lin, C. Investigating flow and heat transfer characteristics in a fuel bundle with split-vane pair grids by CFD methodology. *Ann. Nucl. Energy* **2014**, *64*, 93–99. [[CrossRef](#)]

